Available online at www.sciencedirect.com
ScienceDirect
Applied Mathematical Modelling 33 (2009) 1248–1258
APPLIED MATHEMATICAL MODELLING
www.elsevier.com/locate/apm

Different numerical methods in the study of passive scalar transport in a pipeline x-junction

W. Vicente *, M. Salinas-Vazquez, C. Chavez, E. Carrizosa

Instituto de Ingeniería, Universidad Nacional Autónoma de México, Ciudad Universitaria, 04510 México DF, Mexico

Received 1 April 2006; received in revised form 1 January 2008; accepted 23 January 2008
Available online 8 February 2008

Abstract

A computational fluid dynamic model is used to analyze the transport processes of a passive scalar generated in the mixing of two fluids or flows in a pipeline x-junction. Turbulent flow field is computed for the merging of streams using two and three-dimensional simulations, which are achieved employing Cartesian coordinates, BFC and a cut cell method. These different numerical solving methods are compared. The numerical model is validated through an experimental set-up. Different parameters are measured for various operating conditions. The influence of the angle between pipe inlets is studied to establish the optimal condition in which the passive scalar concentration in both outlets is similar.

Keywords: Concentration; Pipes; Potable water; x-Junction; CFD

1. Introduction

Turbulent mixing of many fluid streams in pipelines is of much interest due to its wide application in industrial and power generation processes. Of particular interest for this work is the study of potable water distribution systems, where water from different sources is mixed. In addition, the dispersion of some disinfectant or polluting substances in the water is also analyzed.

Different T-junction type pipelines have been studied numerically and experimentally [1–4]. However, a reduced number of studies are available for a confined cross-flow, which requires a more complex geometry and turbulent mass transfer simulation. The geometry studied here is a two-pipe configuration with an x-like crossing point. Both pipes transport clean water, but a specified concentration of a passive scalar is added in one of the inlets.

An experimental set-up was designed for this work, consisting of an x-junction with an angle between the two pipe inlets $\alpha = 90°$. The volumetric flow rate in the clean water inlet was varied to study its effect on concentrations in both pipe outlets. The passive scalar used in the experimental set-up represents the hipochlorine

* Corresponding author. Tel.: +52 55 56 23 35x1113; fax: +52 55 56 16 21 64.
E-mail address: wvicenter@ii.unam.mx (W. Vicente).

0307-904X/$ - see front matter © 2008 Elsevier Inc. All rights reserved.
doi:10.1016/j.apm.2008.01.022

in the water. Different parameters were obtained experimentally and results were used for validating the numerical model.

In the numerical model, the hydrodynamics was represented with the Reynolds-averaged continuity, momentum and conservative species equations. The standard $k-\varepsilon$ model [5,6] was used to consider turbulence effects within the flow. The hydrodynamic equations were solved using a finite-volume method.

When flow simulations involve curved geometries or boundaries that are not aligned with the grid orientation, the use of Body-Fitted Coordinates (BFC) or staircase steps approximation in Cartesian coordinates is common. However, many problems are observed, such as: inaccurate results, high computational costs, low accuracy or iteration divergence. As an alternative approach, cut cell methods have become popular, because they have the simplicity and accuracy of the Cartesian coordinates for internal cells (cells with fluid flow), and a more elaborate method only for the boundary surfaces. Many different cut cell methods have been developed, such as: immersed boundary or surface method, embedded boundary method, or the ghost fluid method. In this work, the ASAP method (Arbitrary Source Allocation Procedure) [7,8], which determines the intersections of the complex geometry with the Cartesian grid lines and calculates the free areas and volumes of the partially blocked cells for modifying the transport by source terms, is used.

Considering that numerical simulations give rise to the study of more parameters than those studied experimentally, the present work is only focused on analyzing the influence of the α angle between the pipe inlets in the outlet passive scalar concentrations.

The paper is organized as follows: in the next two sections, the characteristics of the experimental set-up and the numerical model are discussed, and results and performances of different solving methods are compared. Section 4 compares the numerical and experimental results for validation of the mathematical model. In Section 5, the effect of the angle between both pipe inlets over the passive scalar concentration in the outlets is analyzed. Finally, in Section 7, an outline of the most relevant results is presented as conclusion.

2. Experimental set-up

The experimental set-up of the x-junction was designed and constructed in the Hydraulic Laboratory of the Engineering Institute of the National University of Mexico (UNAM). A schematic view of the experimental set-up is shown in Fig. 1. The junction was built in acrylic tube with 90° cross-shaped pipe. The pipe length was 1.23 m with an inner diameter of 0.01905 m (3/4″). The junction had two inlets and two outlets, labeled *inlet1*, *inlet2* and *outlet1, outlet2* respectively. *Inlet1* was supplied with a mixture of clean water and a dye substance, while *inlet2* was delivered with only clean water. Fluid for both inlets was supplied by two storage tanks, provided with one 372.85 W (1/2 HP) pump each. The dye substance was blue ink.

Measurements of volumetric flow rates at the inlets were taken with flow-meters, while at the outlets, volumetric tanks were employed. The concentrations were measured through a Hach spectrophotometer, which employs a color technique in terms of platinum–cobalt units. At the branches, pressure was measured with a piezometer.

Tests were performed for different volume flow rates at *inlet2*. The volume flow rate at *inlet1* was approximately equal to 0.4 dm^3/s for all cases. The Reynolds number (based on mean inlet velocity and pipe diameter) at *inlet1* was $Re = 28{,}000$. The volumetric flow and Reynolds number for *inlet2* varies from 0.30 to 0.80 dm^3/s, and from 23,000 to 50,000, respectively. The experimental uncertainties associated with the measurement of volume flow rates and the concentrations of tracer species were 3% and 4%, respectively.

3. Numerical model

3.1. Numerical procedures

Different procedures were performed to represent the cross-flow. The simplest form is based on a Cartesian grid through the application of porosity, Fig. 2a, where values go from 0, blocked cell, in the solid zone without fluid flow, and 1 in the fluid zone where the entire cell is open to the flow. The second form consists of a BFC grid, where only the flow zone is considered. For this procedure, three different zones were represented and interconnected, Fig. 2b. In Table 1, we present the CPU time and memory used for an example of cross-

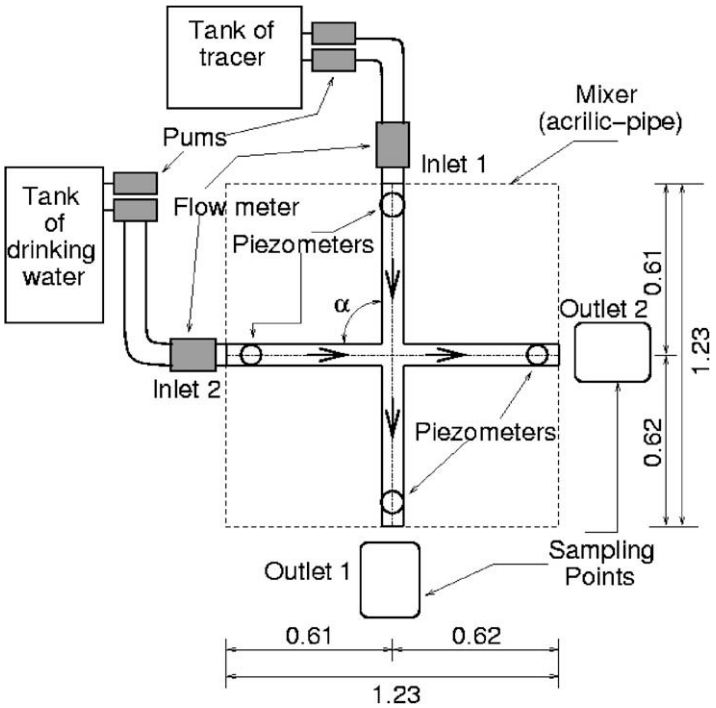

Fig. 1. Experimental set-up.

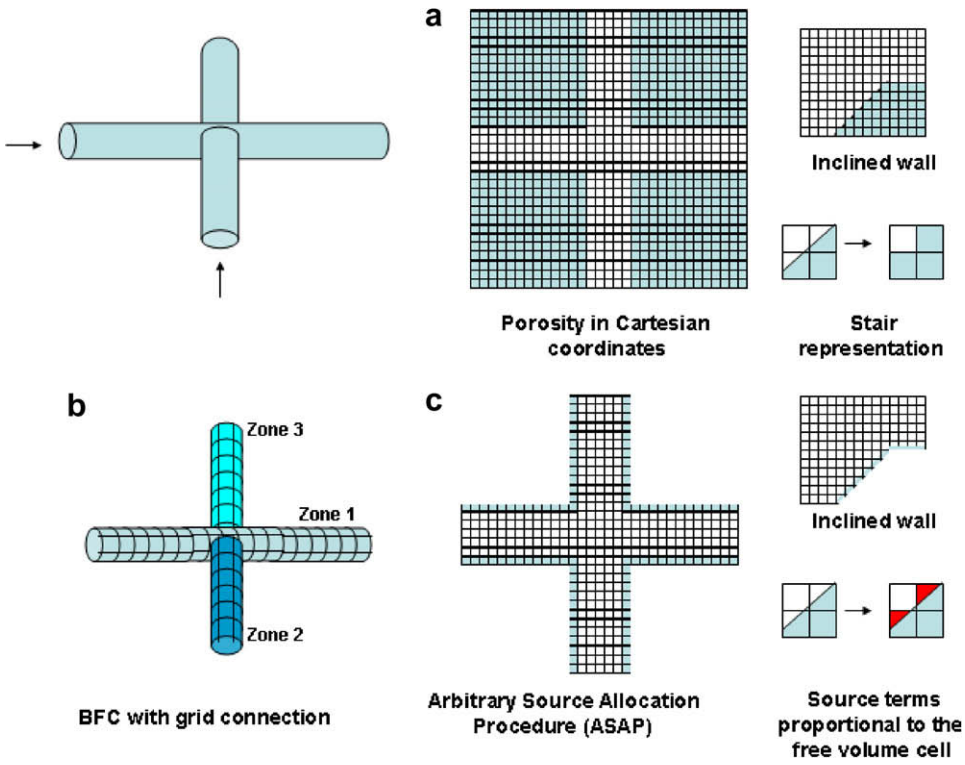

Fig. 2. Different numerical procedures.

Table 1
Numerical results comparison

Numerical method	Cells number	CPU memory (kB)	CPU time (s)
Cartesian	12,100	9.7	153
BFC	2100	12.3	229
ASAP (Cartesian)	12,100	10.3	389

flow with an angle $\alpha = 90°$. The resolution inside the pipes is the same for the three cases. The third case will be explained later. We observed similar results in all cases in velocity and concentration fields and we could not conclude on the best method. However, for the ASAP method, CPU time is more than 2.5 and 1.5 times the CPU time for BFC and Cartesian methods, respectively. These calculations were performed in a PC-Pentium 4 with Windows-XP operative system.

The problems appear when the angle $\alpha \neq 90°$, the connection between pipes is non-orthogonal and/or the walls are not parallel to the Cartesian axis. For the blocking Cartesian grid, the pipe wall is represented in a staircase fashion, Fig. 2c. This wall representation is inadequate and results in an over predicted pressure loss and spurious predictions close the wall.

In the case of the BFC grid, the problem is located in the wall connection, which increases convergence time, or simply makes it impossible to establish converged results (mainly in 3D cases). Due to these problems, and indeed a higher CPU time and memory (not restrictive for a PC-Pentium 4 computer), an alternative procedure was considered, which consists of the use of the ASAP method [7,8]. This is a cut cell method that uses a Cartesian grid for all cells except for those that are intersected by a complex–boundary pipe surface. All the advantages of using the conventional Cartesian grid method are restricted to the internal cells and a more elaborate treatment is only required for the boundary cells. In the cases where a finite volume method was used in this work, the intersections of the complex geometry with the grid lines are determined and the free areas and volumes of the partially blocked cells are calculated, then, the transport equations are modified (for these partially blocked cells) by source terms that account for the local non-orthogonal intersections between the grid and the pipe geometry. This ensures a higher degree of precision and accuracy in representing the walls' true geometry. This method is used in this work for 2D and 3D cases.

3.2. Numerical solution

The cross-flow hydrodynamics was modeled via Reynolds-averaged continuity, momentum and conservative species equations (with the over-bars which usually denote the average dropped for simplicity). The turbulent–convection term, which results from the averaging of the convection term in the conservation equations, was modeled with the standard $k-\varepsilon$ model [5,6].

For the turbulent flow of homogeneous, incompressible, viscous fluid with constant properties, mass and momentum conservation equations in a Cartesian coordinates system may be written as follows [9]:

$$\frac{\partial u_i}{\partial x_i} = 0, \tag{1}$$

$$\frac{\partial u_i}{\partial t} + u_j \frac{\partial u_i}{\partial x_j} = \frac{1}{\rho}\frac{\partial p}{x_i} + \frac{\partial}{\partial x_j}\left[(v + v_t)\frac{\partial u_i}{\partial x_j}\right], \tag{2}$$

where ρ is the fluid density, u_i is the time-average velocity vector, P is the time-average pressure, v is the kinematic viscosity, and v_t is the eddy viscosity. The concentration was modeled through the conservative specie equation:

$$\frac{\partial c}{\partial t} + u_j \frac{\partial c}{\partial x_j} - \frac{\partial}{\partial x_j}\left[\left(\frac{v}{Sc} + \frac{v_t}{\sigma_c}\right)\frac{\partial c}{\partial x_j}\right] = 0, \tag{3}$$

where c is the conservative specie, Sc and Sc_t are the laminar and turbulent Schmidt numbers, respectively. For the present work, the following values were assigned: $\mathrm{Sc} = 1.0$ and $\mathrm{Sc}_t = 0.6$ [10].

3.3. Numerical details

The x-junction was simulated in two and three dimensions. The hydrodynamic equations were solved using a finite-volume method. The mesh in BFC coordinates used for the 2D calculations is shown in Fig. 3. In this geometry, the General Collocated Velocity (GCV) method was used for solving the Navier–Stokes equations [11]. This method uses a segregated pressure-based solver strategy with an additional correction of cell-centre momentum velocity components. The pressure–velocity coupling was based on a linearization which is similar to the well known SIMPLE procedure. The GCV allows the creation of an unstructured multiblock grid from relatively simple structured blocks, which can be generated individually. In the mesh of Fig. 3, three blocks were made and these were linked in the center. When the angle between inlets differed from 90°, two blocks were added to form the joint, avoiding highly non-orthogonal cells.

3D simulations using BFC grids were full of complexities and the grid deformation for $\alpha \neq 90°$ cases did not allow easy convergence of simulations. Cartesian coordinates provide an alternative for the 3D simulations. The Cartesian approach consists of using the ASAP method [7,8]. The ASAP allows to work with complex geometries without creating meshes that are difficult to attain convergence, by the attachment of source terms to the appropriate cells. This simplification was employed for the tri-dimensional simulation of the pipeline x-junction.

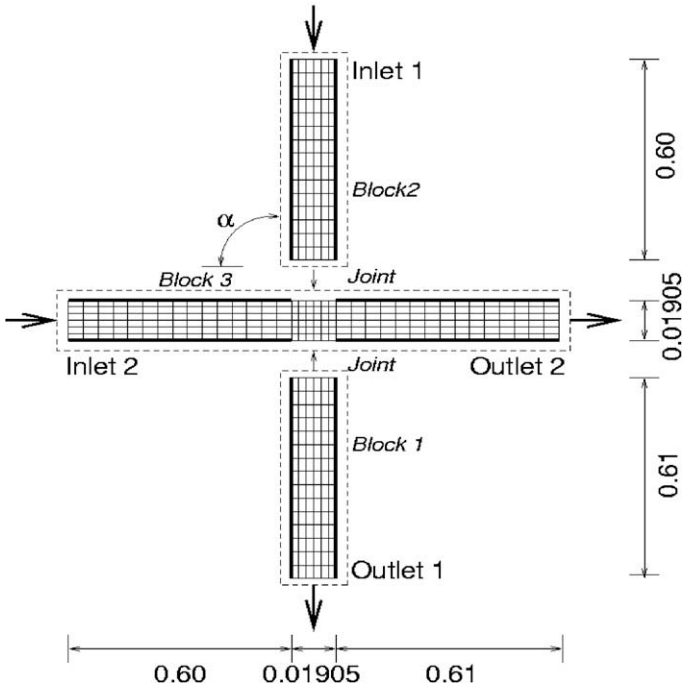

Fig. 3. Numerical grid.

Table 2
Flow characteristics

	2D	3D
Grid points	4200	360,000
Pipes length	1.23 (m)	1.23 (m)
Vol. flow (*inlet1*)	0.43 (dm^3/s)	0.43 (dm^3/s)
Vol. flow (*inlet2*)	0.03–0.82 (dm^3/s)	0.03–0.82 (dm^3/s)
Concentration (*inlet1*)	1.0	1.0
Concentration (*inlet2*)	0.0	0.0

In both cases, BFC and Cartesian grid refinement tests were carried out; the results proved to be grid independent for the above mentioned meshes. The characteristics of simulations are summarized in Table 2.

Flow enters the pipe with a uniform longitudinal velocity. To study the effect of high and low velocities in the passive scalar transport, simulations with inlet volumetric flow values lower than 0.1 and higher than 10.0 dm^3/s are performed. The incoming values of k and ε are calculated from the empirical relations [12]:

$$k_{\text{inlet}} = c_k(0.3u_{\text{inlet}})^2, \tag{4}$$

$$\varepsilon_{\text{inlet}} = c_\varepsilon(0.09^{0.75}k_{\text{inlet}}^{1.5})/(0.1D), \tag{5}$$

where D is the pipe diameter, u_{inlet} is the inlet velocity, c_k and c_ε are constants. The value for both constants in empirical relationships is 1.0. To test whether different inlet k and ε values influence the concentration transport, the constants c_k and c_ε are changed from 0.1 to 10.0.

For simplicity in the presentation of results, several parameters were defined. The predicted mean volumetric flow rate $\mathbf{Q}$ and the mean bulk concentration $\mathbf{C}$ at the outlets are computed as:

$$\mathbf{C} = \frac{\int uc\,\mathrm{d}A}{\int_A u\,\mathrm{d}A}, \tag{6}$$

$$\mathbf{Q} = \int_A u\,\mathrm{d}A, \tag{7}$$

where A is the pipe transversal area, u and c the mean velocity and mean concentration respectively. The inlet and outlet volumetric flows for pipe 1 and 2 are, respectively: $\mathbf{Q}_{i1}$, $\mathbf{Q}_{i2}$, $\mathbf{Q}_{o1}$ and $\mathbf{Q}_{o2}$. They are normalized by the total inlet mean volumetric flow ($\mathbf{Q}_{i1} + \mathbf{Q}_{i2}$). The parameter r_Q is defined as the inlet volumetric flow ratio $r_Q = \mathbf{Q}_{i2}/\mathbf{Q}_{i1}$. Finally, the mean bulk concentrations are normalized by the total inlet mean bulk concentration ($\mathbf{C}_{i1}$).

4. Validation case

Several experimental measurements have been performed for a pipeline x-junction with an angle $\alpha = 90°$ so as to validate the numerical model. Experimental results consisted of mean pressure gradients, concentrations, and volumetric flows.

To test the validity of a 2D approximation, 2D and 3D simulations were performed with the characteristics shown in Table 2. A large number of simulations for much higher and lower volumetric flows than those shown in Table 2 were performed, maintaining similar values of r_Q. The results differ less than 3% from the ones obtained using the original values specified in Table 2. This shows independence of the scalar concentration with the range of the here studied volumetric flows.

The velocity field for the same inlet volumetric flows at both pipes, $r_Q = 1.0$, is illustrated in Fig. 4. The momentum exchange at the junction deforms the velocity profiles and forces the passive scalar toward *outlet2*. In spite of this strong momentum exchange, the mean bulk velocity remains the same before and after the junction in every pipe.

As expected, turbulence increases at the junction and reaches a maximum at the recirculation zone, with the consequent passive scalar mixing. Fig. 5 shows the longitudinal evolution of the mean turbulent kinetic energy. Regardless of the high level of turbulence at the junction zone, here the scalar transport from one pipe to another seems to be independent of it.

This turbulence independence has been tested in simulations with values of k and ε ten times higher and lower than those obtained with the empirical relations, Eqs. (4) and (5). As a result of high turbulence, the concentration is more homogeneous in the fluid just after the junction, but its value remains basically the same at the outlets.

For this validation case, more than 70% of the concentration incoming from *inlet1* is evacuated though *outlet2*. After the junction, the scalar in pipe 1 travels mainly along the high velocity zone. This is illustrated in Fig. 6, where numerical and experimental results show very good agreement.

When the value of r_Q is increased, the flow at *outlet2* is also enhanced, with the corresponding higher concentration values, $\mathbf{C}_{o2}$. $\mathbf{Q}$ and $\mathbf{C}$ profiles at both outlets as a function of r_Q are shown in Fig. 7. A critical point

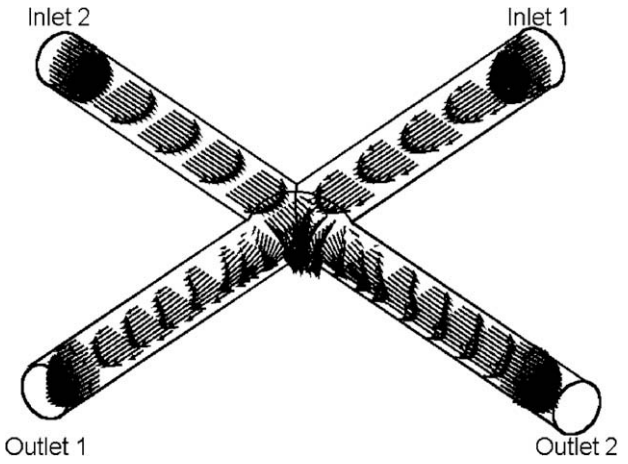

Fig. 4. Velocity vector field for the 3D simulation. $\alpha = 90°$ and $r_Q = 1.0$.

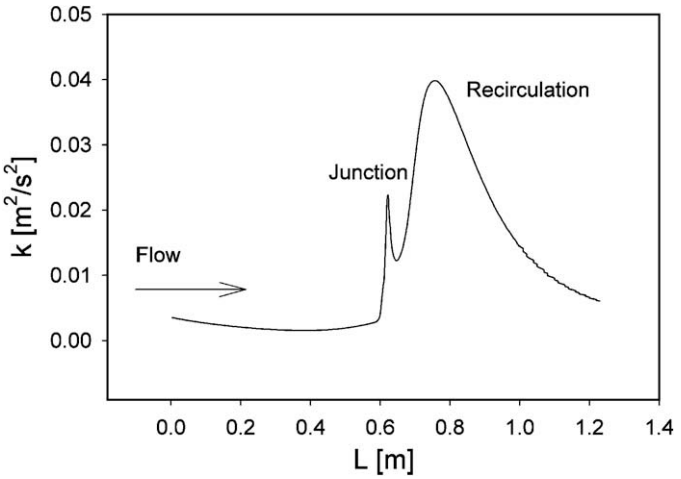

Fig. 5. Validation case, $\alpha = 90°$. Turbulent kinetic energy (k) along pipe2 longitudinal direction, $r_Q = 1.0$.

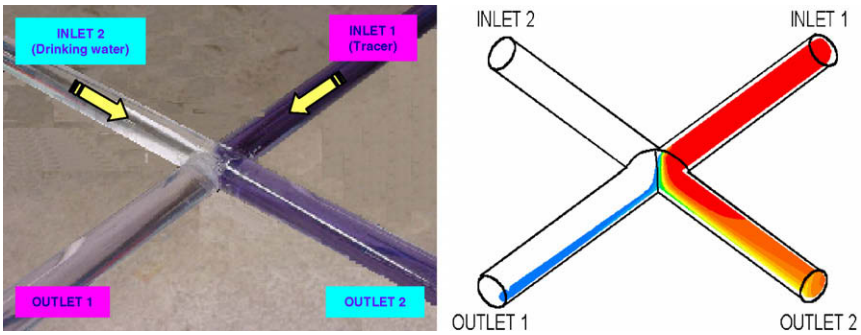

Fig. 6. Validation case, $\alpha = 90°$. Numerical (left) and experimental (right) concentration field. $r_Q = 1.0$.

is observed in Fig. 7-top, where the concentration of both outlets is the same. This point is found for a value $r_Q \approx 0.23$, for an angle $\alpha = 90°$. Working around this point, it is expected to obtain the concentration homogeneity between two flow branches. For many applications, this critical point is of relevant utility.

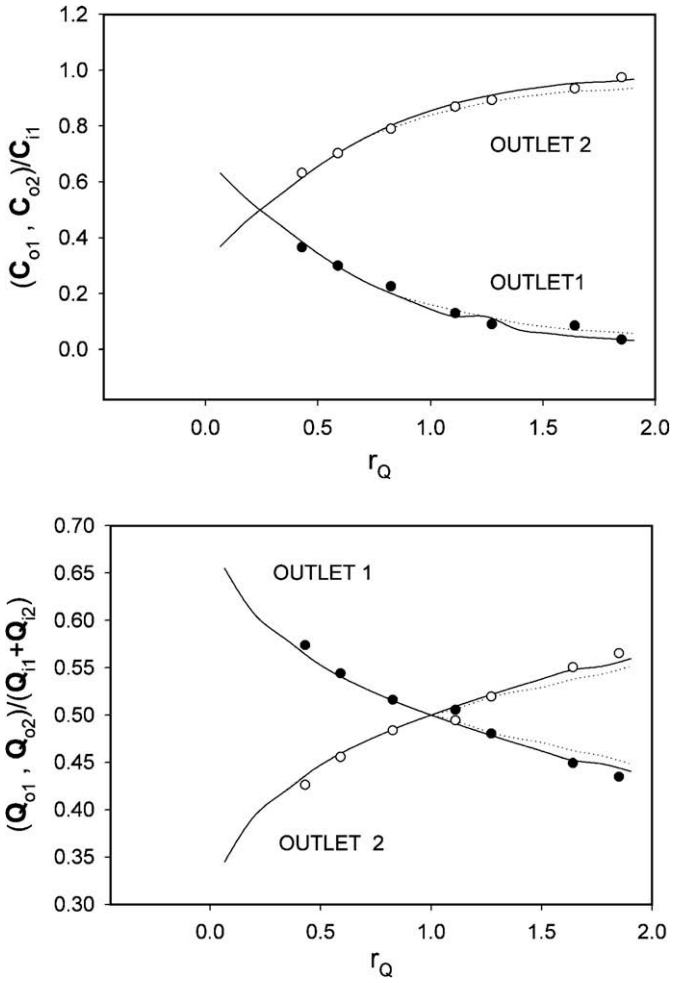

Fig. 7. Validation case, $\alpha = 90°$. Normalized mean bulk concentration (top) and normalized mean volumetric flow (bottom) as a function of r_Q at both outlets. ○ *outlet2* and • *outlet1* experimental data. —— 2D numerical simulation, ····· 3D numerical simulation.

The **Q** profiles show a similar behavior to the **C** profiles. However, the critical point found here, where volumetric flows at both outlets are the same, is displaced to $r_Q = 1.0$, since both pipes transport the same fluid with equal volumetric flow. Analyzing the passive scalar profiles, it may be concluded that most of the fluid evacuated by *outlet2* came through *inlet1* (more than 70%) and vice versa.

The pressure losses, defined as $\Delta P = (P_{\text{inlet}} - P_{\text{outlet}})/P_{\text{inlet}}$, as a function of r_Q, are illustrated in Fig. 8. The difference between both numerical configurations is comparable with measurement errors in experimental data, lower than 4%. Higher differences are mainly found for the highest r_Q values studied. The two dimension approximation proved to be a good way to save computational resources for this kind of study, which requires a high number of numerical data. Just for the validation case, more than 50 simulations were performed. The major discrepancies between numerical and experimental data were found to be lower than 4% in terms of scalar concentration, which establishes the numerical model accuracy.

5. Influence of the junction angle α

As a consequence of the good performance of the numerical model shown in the previous section, the study of configurations with different α angles was achieved considering four other angles: $\alpha = 45°$, 67.5°, 112.5° and 135°. Flow conditions and number of grid points were similar for every case. Only an increase of ≈5% in the

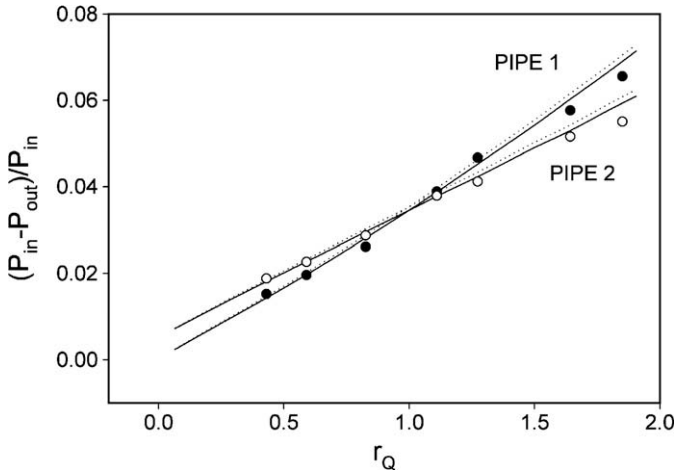

Fig. 8. Validation case, $\alpha = 90°$. Mean pressure loss as a function of r_Q at both pipes. ○ *outlet2* and • *outlet1* experimental data. —— 2D numerical simulation, ····· 3D numerical simulation.

grid resolution at the junction was necessary for cases $\alpha = 45°$ and 135°. The whole range of r_Q values studied for $\alpha = 90°$ was not possible for every angle. For $\alpha = 135°$, convergence was not attained for low and high r_Q values. Many other authors have also reported convergence problems in flows with more than one exit [3], due to mass conservation convergence.

The normalized bulk volumetric flow and passive scalar concentration profiles are shown in Figs. 9 and 10 ($\alpha = 90°$ included) as a function of r_Q. The critical point in the bulk volumetric flow profiles takes place at $r_Q = 1.0$ for every case, although they present profiles with different slopes. The curves with maximum and minimum slope are cases $\alpha = 45°$ and 135°, respectively.

This strong flow interaction is also observed in the passive scalar concentration profiles. For low α values, the concentration at *outlet2* increases substantially. Hence, the concentration at *outlet2* tends to a value close to 1.0 faster. For high α values, this process of passive scalar evacuation by *outlet2* is slower.

For the passive scalar, the value of the critical point, r_{Qcrit}, is not the same for every junction angle. Before this point, *outlet1* transports a higher concentration than that of *outlet2*. After this point, the behavior of the scalar transport is inversed. In Fig. 10, it is possible to observe that as α increases, so does r_{Qcrit} value for crit-

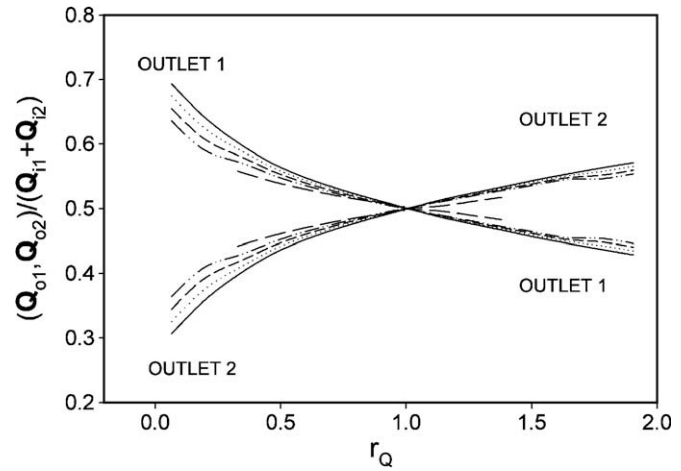

Fig. 9. Different junction angle. Normalized outlet mean volumetric flow as a function of r_Q. —— $\alpha = 45°$; ····· $\alpha = 67.5°$; - - - $\alpha = 90°$; – ·· $\alpha = 112.5°$ and – – $\alpha = 135°$.

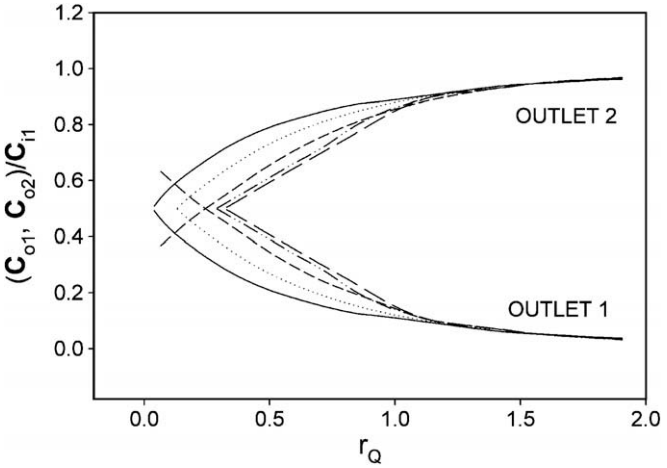

Fig. 10. Different junction angle. Normalized outlet mean concentration as a function of r_Q. —— $\alpha = 45°$; ····· $\alpha = 67.5°$; - - - $\alpha = 90°$; – – $\alpha = 112.5°$ and – – $\alpha = 135$.

ical point in concentration profiles. Accordingly, this r_{Qcrit} value goes from $r_{Qcrit} \approx 0.035$ for $\alpha = 45°$ to $r_{Qcrit} = 0.33$ for $\alpha = 135°$. r_{Qcrit} remains constant to $r_{Qcrit} \approx 0.40$ for high α values ($\alpha > 135°$), see Fig. 11-left. This value was obtained fitting the curve in Fig. 11-left to a logarithmic plot.

These results suggest that working with high α angles is the best option. The inlet volumetric flows shall have the maximum values and the same concentration for both outlets. Pressure losses illustrated in Fig. 11-right provide a clue that should not be overlook in this phenomenon. Pressure losses are much higher with increasing angles. For example, while the increase of r_{Qcrit} from $\alpha = 90°$ to 135° is lower than 30%, the pressure losses are enhanced from 80% to more than 100%. See Fig. 11-right.

Other technical problems could be found in configurations with high α values, such as mechanical vibrations and important normal stresses at the junction. Not only flow characteristics must be considered in the development of a mixing flow system.

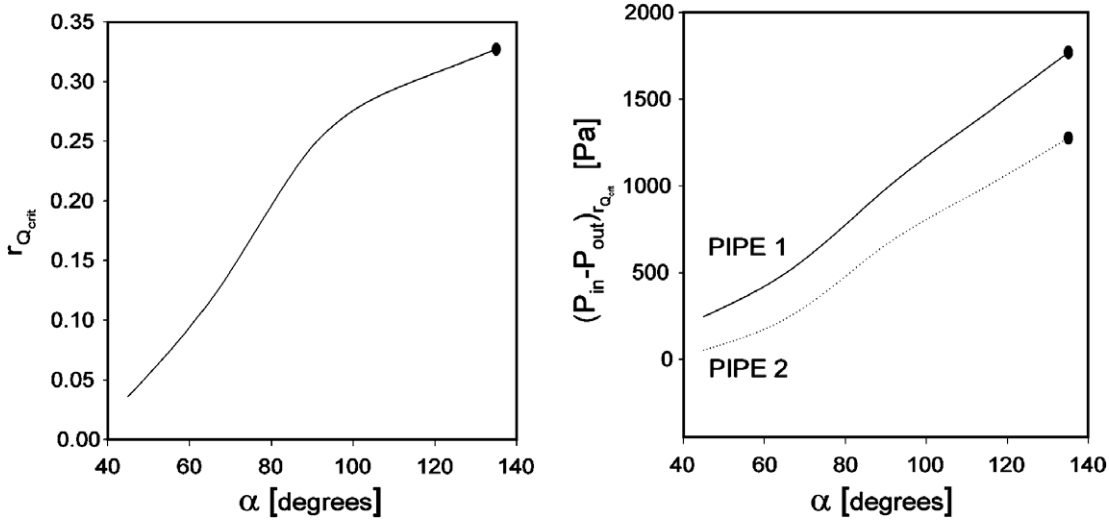

Fig. 11. Different junction angle. Critical value r_{Qcrit}, where concentration in both outlets is the same (left). Pressure losses for the flow in the critical value r_{Qcrit} (right). The value for $\alpha = 135°$ (•) was extrapolated from results.

6. Conclusions

Numerical simulations have been performed with a model employing two- and three-dimensional grids to represent a pipeline x-junction. It has been successively considered an x-junction configuration with an angle between inlets equal to 90°. Comparison between numerical results and experimental data for this configuration shows a very good agreement.

Three different approaches have been used in the computing of turbulent mixing of two streams, i.e. Cartesian grid, body fitted coordinates and the Arbitrary Source Allocation Procedure which implies the use of Cartesian grid.

The ASAP method can be a promising method when complex geometries are required, which can lead to convergence problems caused by the non-orthogonality of cell.

The 2D approximation has shown to be a good approach for saving computational resources for this kind of analysis. For similar results than the 3D configuration, CPU time and the memory used are 20 times lower. This configuration may be of great use when numerous parameters in numerical simulations must be changed. Just for the validation case, more than 50 different simulations were performed. The simulations have been performed in the range $0.02 < r_Q < 2.0$. However, different flow parameters have been tested for determining their influence on the results. These parameters are: inlet kinetic energy, pipe diameter, inlet flow velocity. Differences lower than 4% have been observed between simulations.

Given the good performance of the numerical model, different flow and geometrical parameters could be achieved. For this study, only the junction angle was modified.

For different junction angles, the numerical simulations have shown a critical r_{Qcrit} value, where both outlets transport the same scalar concentration. The critical r_{Qcrit} increases as the junction angle is enhanced. Its maximum value for $\alpha > 135°$ tends to $r_Q \approx 0.4$. With high α angles, pressure losses, vibrations and normal stresses in high junction angles were observed.

References

[1] L.M. Sroka, L.J. Forney, Fluid mixing with a pipeline tee: theory and experiments, AICHE J. 35 (3) (1989) 406–414.
[2] J.B.W. Kok, S. van del Wal, Mixing in T-junctions, Appl. Math. Model. 20 (1996) 232–243.
[3] G. Gan, S.B. Riffat, Numerical determination of energy losses at duct junctions, Appl. Eng. 67 (2000) 331–340.
[4] D. Lee, J.Y. Chen, Numerical simulation of flow fields in a tube with two branches, J. Biomech. 33 (2000) 1305–1312.
[5] B.E. Launder, D.B. Spalding, The numerical computation of turbulent flows, Comput. Meth. Appl. Mech. Eng. 3 (1974) 269–289.
[6] W.P. Jones, B.E. Launder, The prediction of laminarisation with a two-equation model of turbulence, Int. J. Heat Mass Tran. 15 (1972) 301–314.
[7] H. Ji, F.S. Lien, E. Yee, An efficient second-order accurate cut-cell method for solving the variable coefficient poisson equation with jump condition on irregular domains, Int. J. Numer. Meth. Fluid 52 (2006) 723–748.
[8] D.R. Parsons, G.F.S. Wiggs, I.J. Walker, R.I. Ferguson, B.G. Garvey, Numerical modelling of airflow over an idealised transverse dune, Environ. Modell. Softw. 19 (2004) 153–162.
[9] X. Wang, Z. Feng, L.J. Forney, Computational simulation of turbulent mixing with mass transfer, Comput. Struct. 70 (1999) 447–465.
[10] A.J. Reynolds, The prediction of turbulent Prandtl and Schmidt number, Int. J. Heat Mass Tran. 18 (9) (1975) 1055–1069.
[11] I.N. Poliakov, V.A. Semin, Development and evaluation of new linear equation solvers for PHOENICS, The PHOENICS J. Comput. Fluid Dynam. Appl. 7 (1) (1994) 34–57.
[12] M.B. Abbot, D.R. Basco, Computational Fluid Dynamics: An Introduction for Engineers, Longman Scientific and Technical John Wiley and Sons, 1989.